Supplementary Information

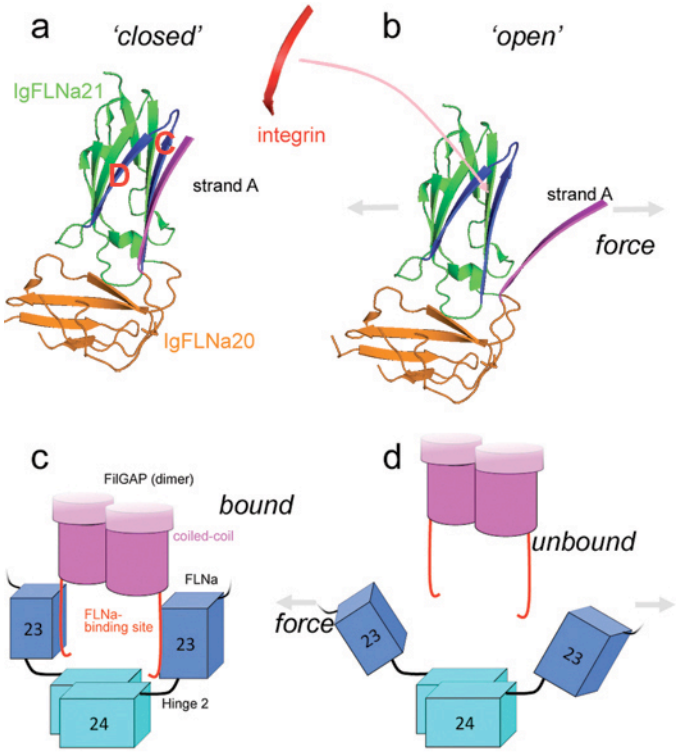

Supplemental Figure S1: Model of mechanosensitive integrin and FilGAP binding to FLNa.

A molecular model of the force-mediated interaction between FLNa Ig repeats 20 and 21 which allows integrin to bind is presented in panels a and b. When FLNa is unstressed, strand A of IgFLNa repeat 20 (purple) partially covers neighboring repeat 21 (green) between strands C and D (blue), as shown in panel a. The application of force moves strand A from repeat 21, uncovering the binding site for integrin (red) allowing it to bind the cryptic site (panel b). FilGAP (purple) binds to unstressed FLNa (blue) by binding both of the IgFLNa23 repeats simultaneously as shown in panel c. Stretching FLNa spatially separates these repeats from each other, preventing FilGAP from simultaneously binding both, thus losing its avidity and unbinding from FLNa as shown in panel d.

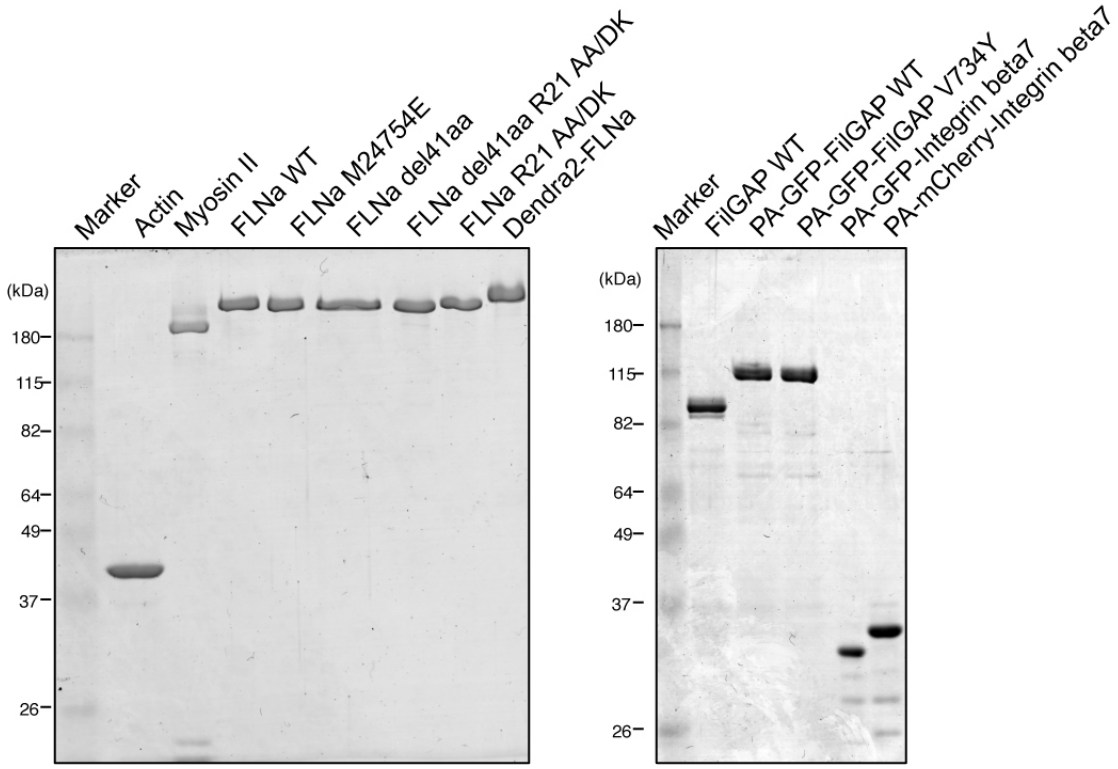

Supplementary Figure S2: SDS-PAGE gel showing purified proteins used in this study.

Proteins were prepared in accordance with standard techniques and those outlined in the supplemental information methods section. After purification, proteins were examined by SDS-PAGE to determine purity, and stained with CBB.

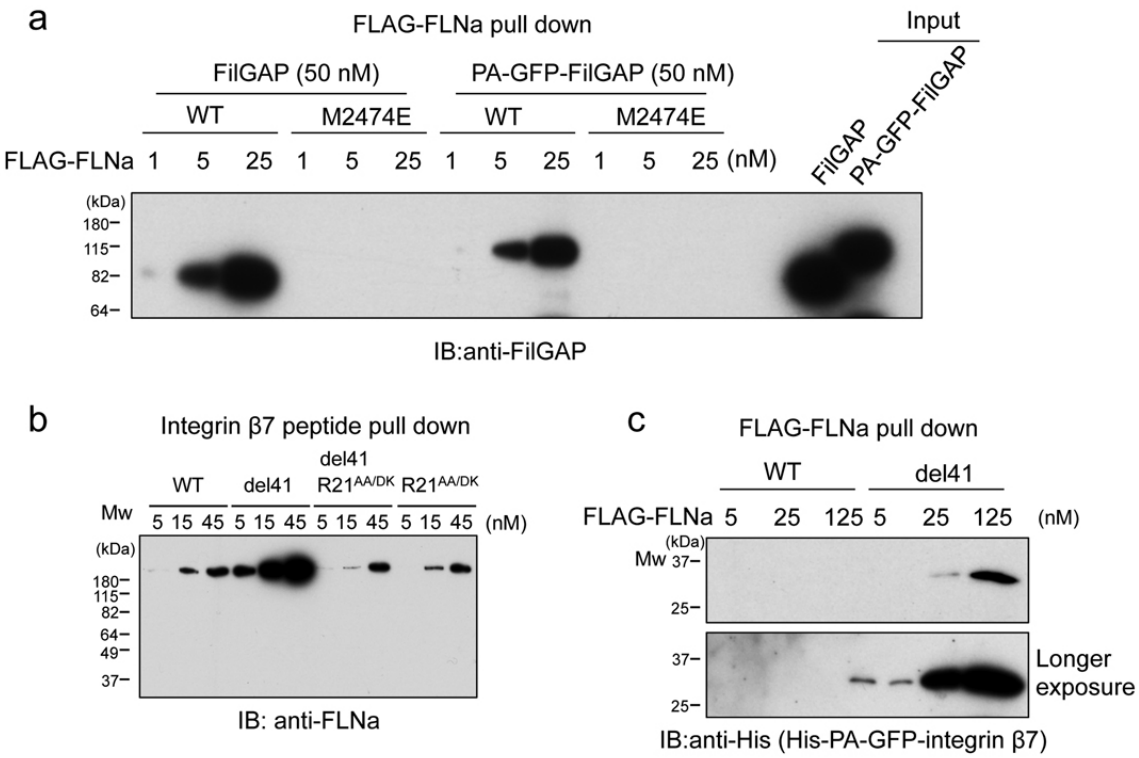

Supplementary Figure S3: PAFP conjugation does not affect FilGAP or Integrin FLNa binding kinetics

a) Binding of FilGAP and PA-GFP-FilGAP to FLNa. Full-length FilGAP and PA-GFP-FilGAP (50nM each) were pulled down with increasing amounts of wild-type (WT) and mutant (M2474E) FLAG-FLNa. The FLAG-FLNa were immunoprecipitated with FLAG-specific mAb immobilized on agarose beads. Bound FilGAP was detected by immunoblotting using rabbit pAbs to FilGAP.

b) Deletion of 41aa exposes integrin β7 binding site. Synthetic peptide of integrin β7 cytoplasmic domain (Cys-^{771}KQDSNPLYKSAITTTINPR^{789}) was immobilized on Sulfo-Link agarose beads and mixed with increasing amounts of wild-type and mutant (del41, residues 2126-2167 aa are deleted and the ligand binding site is constitutively exposed; AA/DK, A2272D/A2274K) FLNa. Bound FLNa was detected by immunoblotting using mouse mAb to FLNa. c) Binding of PA-GFP integrin beta7 cytoplasmic domain (769-789aa) to FLNa. PA-GFP-integrin beta7 (200nM each) were pulled down with increasing amounts of wild-type (WT) and mutant (del41) FLAG-FLNa. The FLAG-FLNa were immunoprecipitated with FLAG-specific mAb immobilized on agarose

beads. Bound His-PA-GFP-integrin β7 was detected by immunoblotting using His-tag mAb conjugated with horseradish peroxidase.

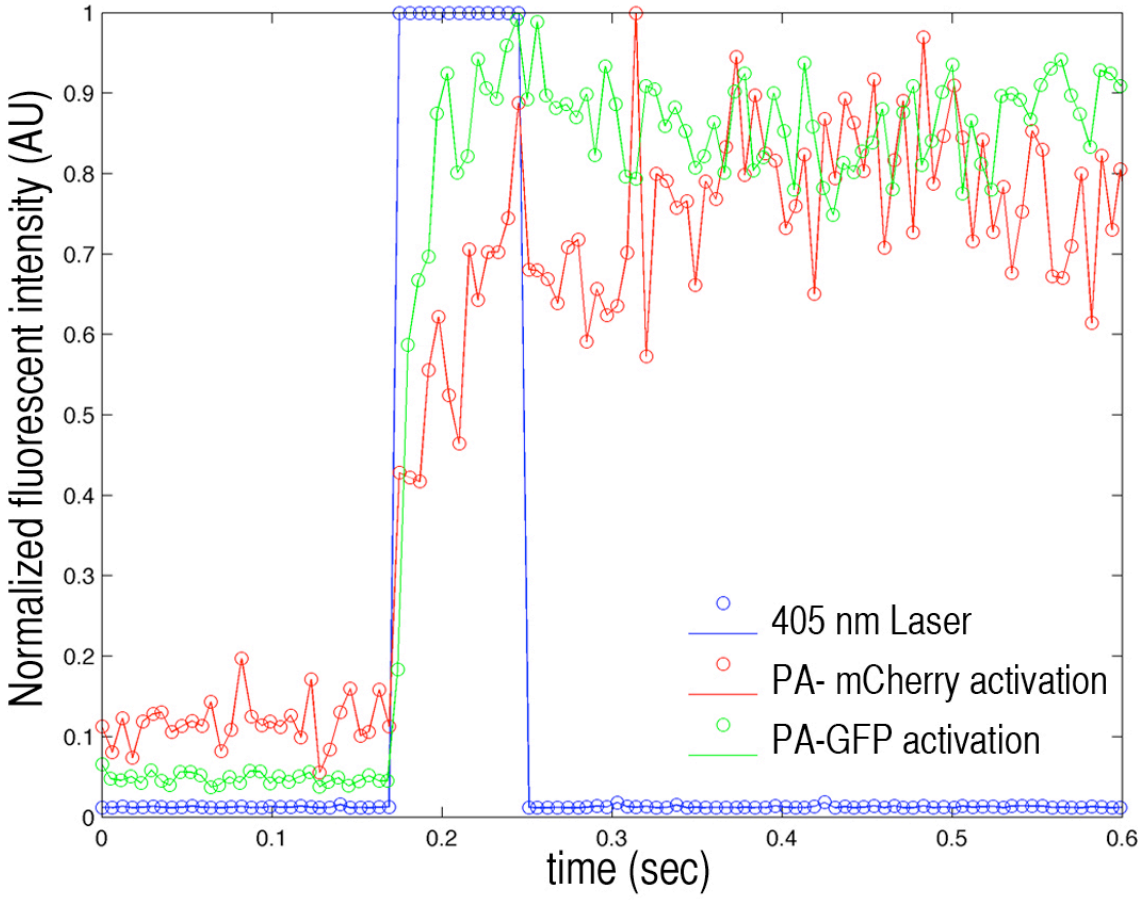

Supplemental Figure S4: Photoactivation times for PA-GFP and PA-mCherry. PA-GFP (green) or PA-mCherry (red) adsorbed to glass are used to demonstrate the photoactivation time after exposure to a 50 ms 405 nm light pulse (blue). PA-GFP reaches maximum activation within ~ 25 ms, whereas PA-mCherry is somewhat slower, occurring over ~ 120 ms. Images were acquired every 5 ms.

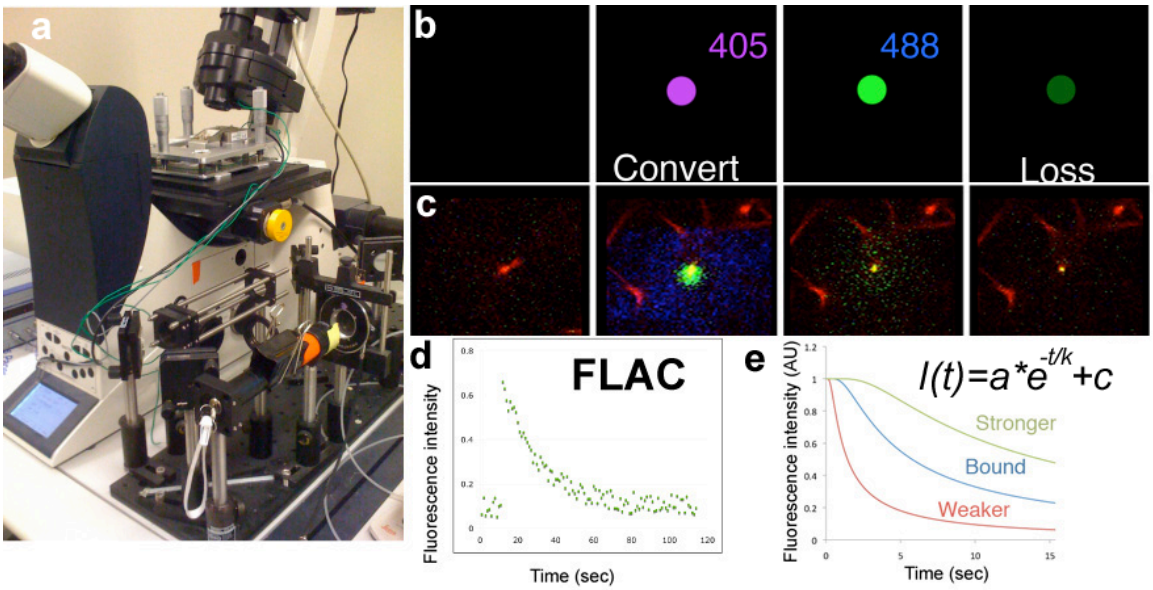

Supplemental Figure S5: Experimental description of Fluorescence Loss After photoConversion (FLAC) for quantitative binding measurements.

a) The experimental platform for FLAC is a Leica SP5 confocal with an external 405 laser (Bestofferbuy.com China), a telescope to expand the beam, and a shutter to control the pulse of light used in photoactivation. On the microscope stage is the piezo-driven shear cell used for external shear measurements. b) In FLAC, an initially dark sample containing PAFPs is pulsed with 405 nm light, causing an irreversible change to the PAFPs which increases their fluorescence by orders of magnitude. As fluorophores unbind and diffuse, the fluorescence intensity decreases, as demonstrated in c), where PA-GFP ß7 integrin unbinds and diffuses in an F-actin-FLNa network (see supplemental movie 1). d) This fluorescence decrease follows a general exponential decay, and this decay is slower when the PAFP is more tightly bound within the sample. e) The difference in exponential decay between tightly or weakly bound PAFP constructs is illustrated, and a single exponential equation, $I(t)=a*e^{(-t/k)}+c$, is used to fit data and determine the time-constant, k, which is the characteristic unbinding time.

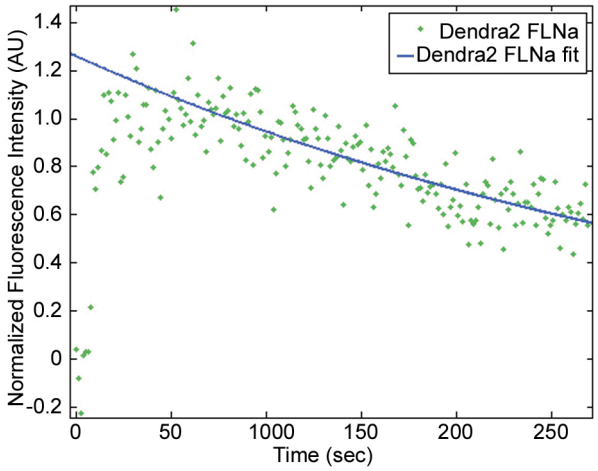

Supplemental Figure S6: FLAC based measurement of FLNa turnover time in F-actin-FLNa networks.

0.12 µM Dendra2-conjugated FLNa was mixed with 24 µM F-actin and allowed to polymerize with 1x F-buffer for 2 hours. After a 50 ms 405 nm laser pulse is applied, the Dendra2-FLNa converts to red fluorescence, the intensity of which decays in time as FLNa unbinds and diffuses. Fitting the exponential decay of fluorescence with $I(t)=a*e^{(-t/k)}+c$ reveals a characterisitic unbinding time-constant, k, of approximately 390 s, demonstrating that FLNa crosslinks unbind and rebind on the time-scale of approximately 6 minutes.

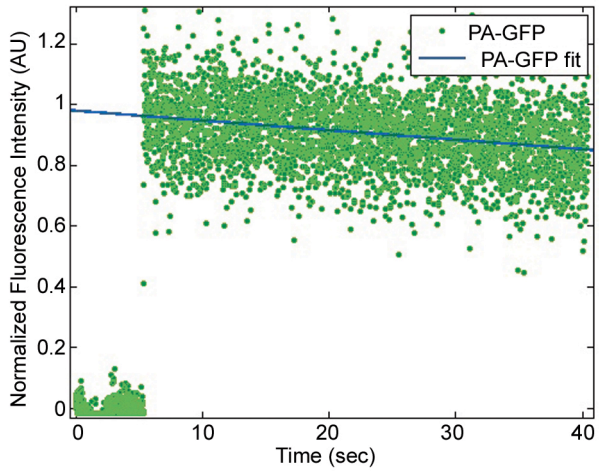

Supplemental Figure S7: Photobleaching of PAFPs occurs on timescales longer than minutes.

PA-GFP non-specifically adsorbed onto glass was photo-activated and the fluorescence intensity was monitored, providing the time-dependent photo-bleaching due to imaging the sample in FLAC experiments. The vertical axis represents fluorescence intensity in normalized arbitrary units, and the horizontal axis shows time in seconds. Data has been normalized such that pre-activation averages to zero intensity, and maximum intensity average is set to 1. On the time scale relevant to FLAC-based binding studies (<10s), photobleaching is negligible. PA-GFP fluorescence data was fit exponentially to $I(t)=a*e^{(-t/k)}+c$, yielding a time constant, k, of approximately 800s.

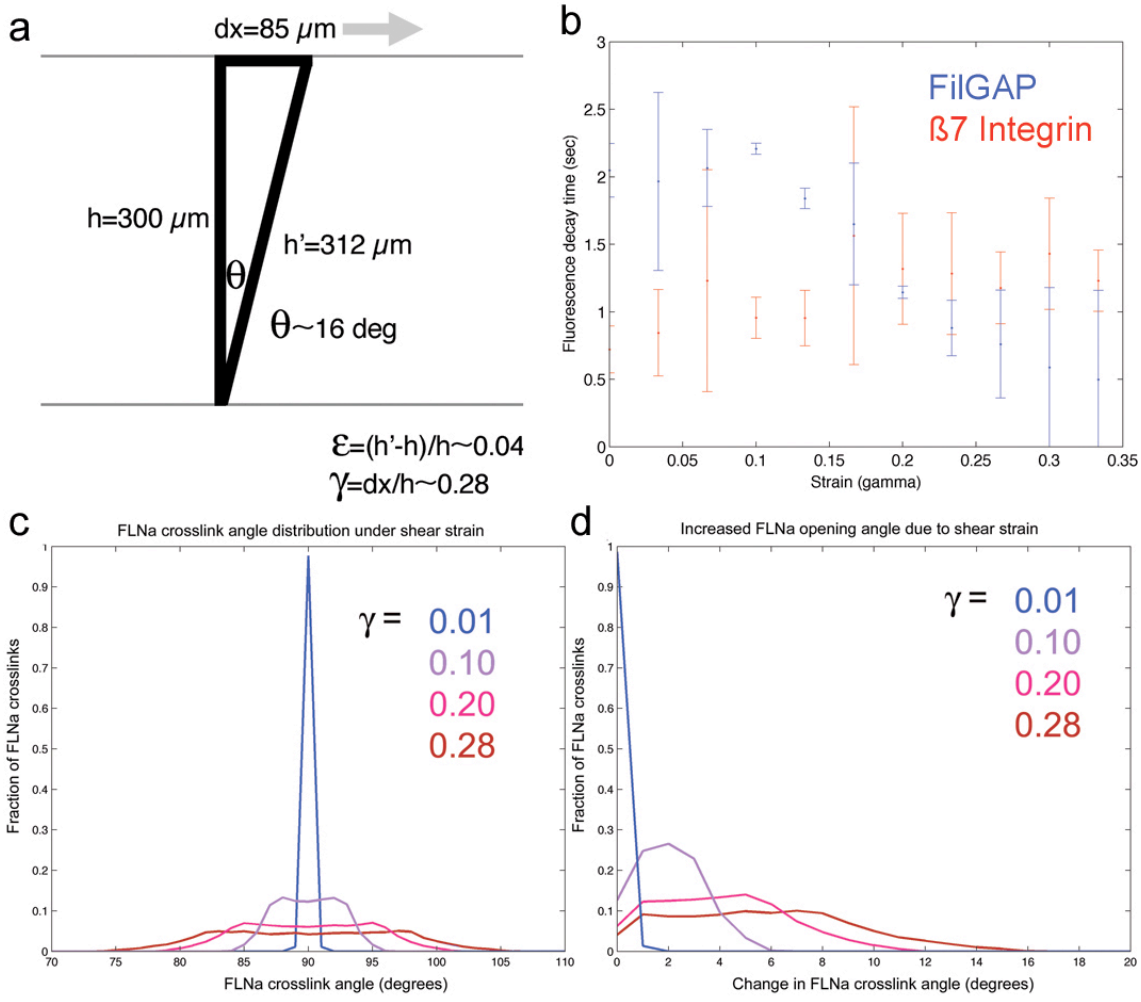

Supplemental Figure S8: Effect of shear on an orthogonal crosslinked network.

a) Scale illustration of the deformation applied to actin-FLNa networks by the shear cell apparatus. A 300 μm gap, *h*, separates the lower and upper plate. The lower plate is held fixed, while the upper plate is linearly moved 85 μm, *dx*, by a piezo-actuator. This displacement shears the sample, deforming the network and stretching the system by 4%

(engineering strain). This deformation also shifts the network by an angle of 16 degrees, corresponding to a shear strain, γ, of 0.28. b) Fluorescence decay time as a function of strain applied by uniaxial shear causes FilGAP (blue) to bind less and ß7 integrin (red) to bind more. c) MatLAB Monte-Carlo simulation of the change in angle distribution for a random distribution of orthogonal crosslinkers such as FLNa in 3D space under uniaxial strain. The distribution remains centered about 90 degrees, however, it is spread to a larger variation in angles due to the shear transformation as a function of random fiber angles. d) Corresponding simulated increase in opening angle of FLNa crosslinks in response to a uniaxial shear strain. Here only the positive (i.e. increasing change in opening angles) are plotted, representing the half of the distribution expected to contribute to mechanotransduction, particularly in the case of FilGAP. The weighted mean increase in angle at γ=0.28 is ~6.1 degrees.

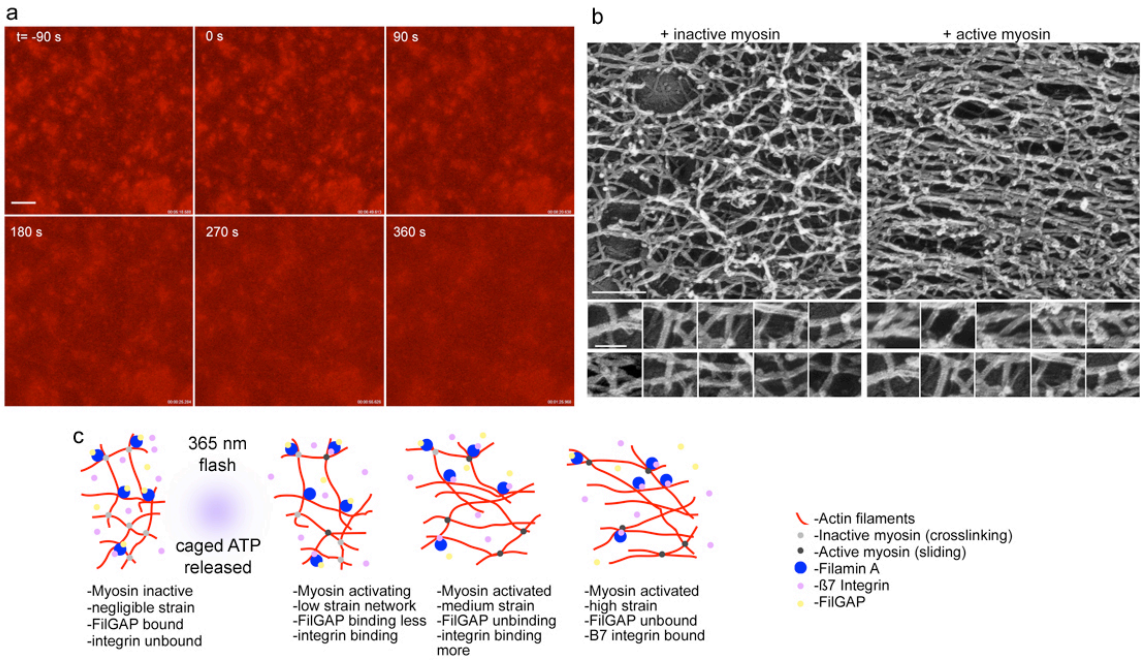

Supplemental Figure S9 Myosin II contraction stresses and deforms FLNa in F-actin-FLNa-myosin networks.

a) Alexa 546 phalloidin labeled actin structures are seen to homogenize after a flash of 365 nm light releases ATP (see also supplemental movie 3). 20 µm scale. b) Electron micrograph of acto-myosin network with blebbistatin used to inactivate contractile activity. Scale bar in upper panel is 200 nm, in lower panel 50 nm. c) F-actin FLNa networks with Myosin II and FilGAP or integrin are allowed to exhaust their ATP and

come to rest in an unstressed-FLNa equilibrium state. When fresh ATP is introduced by uncaging photolabile ATP, myosin resumes contraction and stresses the network. When FLNa is deformed by active myosin, FilGAP dissociates while ß7 integrin binds with higher affinity.

Supplemental Movie Captions

Supplemental movie S1mov

PA-GFP ß7 Integrin binds longer to del41 mutant FLNa than wild type FLNa.

12 uM actin networks with 0.24 uM FLNa (1:50 actin:FLNa) were assembled with 50 nM PA-GFP ß7 integrin constructs. This higher FLNa:actin ratio induces network bundling, however, it is useful in demonstrating the FLAC differences through visible images rather than solely quantifying fluorescence levels. S1mov is 2x real-time, and each fluorescent image sequence is 24 μm across. F-actin is shown in red, the PAFP activating flash in blue, and the PAFP in green. Movie S1mov shows PA-GFP ß7 integrin with wild type FLNa (upper left) and d41 FLNa (upper right), which has the cryptic binding site of repeat 21 constitutively open. The lower panel quantitatively compares the fluorescence decay of the PA-GFP ß7 integrin, demonstrating the higher binding affinity of ß7 integrin to the d41 FLNa mutant (red) over wild-type FLNa (blue), with the vertical axis presenting fluorescence intensity in normalized arbitrary units, and the horizontal axis shows time in seconds. Data has been normalized such that pre-activation averages to zero intensity, and maximum intensity is set to 1. Fluorescence data was fit exponentially to $I(t)=a*e^{(-t/k)}+c$, yielding time constants, k, of 2.2 s for PA-GFP ß7 integrin binding to wild type FLNa, and 5.4 s for binding to the d41 FLNa mutant.

Supplemental movie S2mov

PA-GFP FilGAP binds longer to wild-type FLNa than to M2474E mutant FLNa.

12 uM actin networks with 0.24 uM FLNa (1:50 actin:FLNa) were assembled with 50 nM PA-GFP FilGAP. This higher FLNa:actin ratio induces network bundling, however,

it is useful in demonstrating the FLAC differences through visible images rather than solely quantifying fluorescence levels. S2mov is 2x real-time, and each fluorescent image sequence is 24 μm across. F-actin is shown in red, the PAFP activating flash in blue, and PA-GFP FilGAP in green. M2474E mutant FLNa (upper left) lacks the binding site for FilGAP at repeat 23, while wild-type FLNa (upper right) retains this binding site. The lower panel quantitatively compares the fluorescence decay of the PA-GFP FilGAP, demonstrating the lower binding affinity of FilGAP to the M2474E mutant FLNa (red) over wild-type FLNa (blue), with the vertical axis presenting fluorescence intensity in normalized arbitrary units, and the horizontal axis shows time in seconds. Data has been normalized such that pre-activation averages to zero intensity, and maximum intensity is set to 1. Fluorescence data was fit exponentially to $I(t)=a*e^{(-t/k)}+c$, yielding time constants, k, of 5.1 s for PA-GFP FilGAP binding to wild type FLNa, and 0.9 s for binding to the M2474E FLNa mutant.

Supplemental movie S3mov

Myosin II deforms actin networks when ATP is available.

24μM actin was polymerized in the presence of 0.12 μM FLNa, 1μM Myosin II, 2.5mM ATP, and 2mM caged ATP. All of the original 2.5mM ATP had been consumed over a period of six hours, and FLNa stress within the network was dissipated by FLNa unbinding and rebinding in unstressed configurations. At video time 7:19.955 the sample is exposed to a 4 s flash of 50 mW of 365 nm light, releasing the 2mM of caged ATP, which immediately begins to activate myosin. Myosin contractility resumes and the network appears uniform after approximately 5 minutes. This process is illustrated in Fig S9, highlighting the stretching of FLNa by myosin contractility, and the resulting binding of integrin and unbinding of FilGAP.